EGFR Blockade Reverts Resistance to KRAS^{G12C} Inhibition in Colorectal Cancer

Vito Amodio[1,2], Rona Yaeger[3], Pamela Arcella[1,2], Carlotta Cancelliere[1], Simona Lamba[1], Annalisa Lorenzato[1,2], Sabrina Arena[1,2], Monica Montone[1], Benedetta Mussolin[1], Yu Bian[4], Adele Whaley[4], Marika Pinnelli[1,2], Yonina R. Murciano-Goroff[3], Efsevia Vakiani[5], Nicola Valeri[6,7], Wei-Li Liao[8], Anuja Bhalkikar[8], Sheeno Thyparambil[8], Hui-Yong Zhao[4,9], Elisa de Stanchina[4,9], Silvia Marsoni[10,11], Salvatore Siena[10,12], Andrea Bertotti[1,2], Livio Trusolino[1,2], Bob T. Li[3,13], Neal Rosen[4,14], Federica Di Nicolantonio[1,2], Alberto Bardelli[1,2], and Sandra Misale[4]

ABSTRACT

Most patients with *KRAS*^{G12C}–mutant non–small cell lung cancer (NSCLC) experience clinical benefit from selective KRAS^{G12C} inhibition, whereas patients with colorectal cancer bearing the same mutation rarely respond. To investigate the cause of the limited efficacy of KRAS^{G12C} inhibitors in colorectal cancer, we examined the effects of AMG510 in *KRAS*^{G12C} colorectal cancer cell lines. Unlike NSCLC cell lines, *KRAS*^{G12C} colorectal cancer models have high basal receptor tyrosine kinase (RTK) activation and are responsive to growth factor stimulation. In colorectal cancer lines, KRAS^{G12C} inhibition induces higher phospho-ERK rebound than in NSCLC cells. Although upstream activation of several RTKs interferes with KRAS^{G12C} blockade, we identify EGFR signaling as the dominant mechanism of colorectal cancer resistance to KRAS^{G12C} inhibitors. The combinatorial targeting of EGFR and KRAS^{G12C} is highly effective in colorectal cancer cells and patient-derived organoids and xenografts, suggesting a novel therapeutic strategy to treat patients with *KRAS*^{G12C} colorectal cancer.

SIGNIFICANCE: The efficacy of KRAS^{G12C} inhibitors in NSCLC and colorectal cancer is lineage-specific. RTK dependency and signaling rebound kinetics are responsible for sensitivity or resistance to KRAS^{G12C} inhibition in colorectal cancer. EGFR and KRAS^{G12C} should be concomitantly inhibited to overcome resistance to KRAS^{G12C} blockade in colorectal tumors.

See related commentary by Koleilat and Kwong, p. 1094.

[1]Candiolo Cancer Institute, FPO - IRCCS, Candiolo, Torino, Italy. [2]Department of Oncology, University of Torino, Candiolo, Torino, Italy. [3]Department of Medicine, Memorial Sloan Kettering Cancer Center, New York, New York. [4]Molecular Pharmacology Program, Memorial Sloan Kettering Cancer Center, New York, New York. [5]Department of Pathology, Memorial Sloan Kettering Cancer Center, New York, New York. [6]Center for Evolution and Cancer, The Institute of Cancer Research, London, United Kingdom. [7]Department of Medicine, The Royal Marsden Hospital, London, United Kingdom. [8]mProbe Inc., Rockville, Maryland. [9]Antitumour Assessment Core Facility, Memorial Sloan Kettering Cancer Center, New York, New York. [10]Niguarda Cancer Center, Grande Ospedale Metropolitano Niguarda, Milan, Italy. [11]Istituto FIRC di Oncologia Molecolare (IFOM), Milan, Italy. [12]Department of Oncology and Hemato-Oncology, University of Milan, Milan, Italy. [13]Weill Cornell Medical College, New York, New York. [14]Center for Molecular-Based Therapy, Memorial Sloan Kettering Cancer Center, New York, New York.

Note: Supplementary data for this article are available at Cancer Discovery Online (http://cancerdiscovery.aacrjournals.org/).

V. Amodio, R. Yaeger, and P. Arcella are co–first authors of this article.

A. Bardelli and S. Misale are co–last authors of this article.

Corresponding Authors: Sandra Misale, Memorial Sloan Kettering Cancer Center, 408 E 68th Street, New York, NY 10065. Phone: 347-839-0728; E-mail: misales@mskcc.org; and Alberto Bardelli, Candiolo Cancer Institute, FPO - IRCCS, Department of Oncology, and University of Torino, Strada Provinciale 142, km 3.95, Candiolo 10060, Torino, Italy. Phone: +39-01-1-993-3235; E-mail: alberto.bardelli@unito.it

Cancer Discov 2020;10:1129–39

doi: 10.1158/2159-8290.CD-20-0187

INTRODUCTION

The small GTPase KRAS is mutated and constitutively active in 15% of all human tumors (1). This protein acts as a molecular switch, transitioning from an active (GTP-bound) to an inactive (GDP-bound) state. This transition is highly regulated, and physiologic feedback loops limit the duration of KRAS activation. Guanine exchange factors, such as SOS1, and GTPase activating proteins (GAP), such as NF1, directly mediate KRAS activation (2, 3). When mutated, KRAS loses the ability to interact with GAPs and therefore becomes constitutively activated, driving downstream MAPK and PI3K–AKT signaling pathways and enhancing cancer cell proliferation and survival (4). Different mutations in KRAS may modify the intrinsic activation (GTP-bound state) of the mutant protein and its interaction with downstream effectors, such as RAF proteins (5, 6). Moreover, KRAS signaling is also regulated by negative feedback mechanisms through the transcriptional induction of protein phosphatases (DUSPs and Sproutys) and SPREDs (2). The complexity of the signaling network and the heterogeneous features of the multiple *KRAS*-mutant alleles have contributed to the difficulty in developing molecularly targeted therapies against mutant KRAS, a target considered undruggable for decades.

However, in recent years, the unique characteristics of one of the KRAS-mutant alleles, KRAS^{G12C}, have been exploited for the design of covalent inhibitors that can specifically bind the cysteine on the mutant residue (7). These inhibitors can bind G12C-mutant KRAS beneath the effector binding switch II domain when KRAS is in the GDP-bound (inactive) state, trapping KRAS in its inactive form and taking advantage of the retained, intrinsic cycling of the G12C mutant from GTP-bound to GDP-bound states (7, 8). Given this particular feature of the KRAS^{G12C}-mutant protein, the efficacy of these compounds can be increased by concomitant receptor tyrosine kinase (RTK) inhibition that further maintains KRAS^{G12C} in a GDP-bound conformation, facilitating the binding of the covalent inhibitor (7–9).

Besides RTK inhibition, several other combinatorial strategies have already been proposed, with the goal of potentiating the effects of these inhibitors (10–13). Importantly, the unique feature of KRAS^{G12C} covalent inhibitors, which only bind the mutant allele, renders these drugs a potentially ideal partner for combinatorial strategies, as toxicities should be minimized and limited to the combinatorial partner.

Several clinical trials testing the efficacy of KRAS^{G12C}-targeted drugs are currently ongoing, and early results from the first two trials using AMG510 and MRTX849 have documented promising outcomes in the clinic. However, clinical studies unexpectedly reported that the response rate to these drugs is high in patients with non–small cell lung cancers (NSCLC) but limited in patients with colorectal cancer (14, 15).

In this work, we sought to understand the mechanisms underlying this lineage difference. We hypothesized that NSCLC bearing *KRAS*^{G12C} could be intrinsically different from *KRAS*^{G12C}-mutant colorectal cancer, despite harboring the same oncogenic mutation. We and others previously reported that *BRAF*^{V600E} colorectal cancer has limited sensitivity to single-agent RAF inhibitors, and this is a result of an adaptive response selectively triggered in colorectal cancer (16–18).

Therefore, we examined the adaptive response to KRAS^{G12C} inhibition and its kinetics in *KRAS*^{G12C}-mutant NSCLC and colorectal cancer cell models. We show that *KRAS*^{G12C}-mutant colorectal cancers maintain sensitivity to upstream RTK signaling, particularly EGFR. Using biochemical and pharmacologic approaches, we show that EGFR reactivation restricts the efficacy of KRAS^{G12C} inhibition in colorectal cancer. We find that KRAS^{G12C} and EGFR blockade is effective to overcome this adaptive resistance, both in cell lines and in patient-derived models. These findings have immediate relevance for clinical strategies to overcome unresponsiveness to KRAS^{G12C} blockade in patients with colorectal cancer.

RESULTS

ERK Inhibition Is Not Sustained in Colorectal Cancer Cell Lines Treated with AMG510

To understand the mechanistic basis for differential clinical responses to treatment with the selective KRAS^{G12C} inhibitor AMG510 in colorectal cancer and NSCLC, we analyzed the effect of this drug in a panel of *KRAS*^{G12C}-mutant cell lines. These included two NSCLC (NCIH358 and LU65) and seven colorectal cancer (C106, RW7213, SW837, SNU1411, JVE015, and LIM2099) cell lines. Response to AMG510 was measured in a dose–response proliferation assay. Sensitivity to single agent was comparable among the models, showing no clear difference between colorectal cancer and NSCLC cell lines (Fig. 1A). Therefore, to explore the quality, duration, and adaptive signaling response to drug treatment, we compared the NSCLC cell lines with four colorectal cancer models, consisting of two representative models with low IC_{50} to AMG510 (C106 and RW7213) and two representatives with high IC_{50} values (SW837 and SNU1411). Cells were subjected to increasing concentrations of AMG510 for 1 and 24 hours (Fig. 1B). After 1 hour of drug treatment, KRAS^{G12C} inhibition led to downregulation of phosphorylated ERK in a dose-dependent manner in all cell models, regardless of tumor lineage. However, after 24 hours of drug exposure, we observed that both NSCLC cell lines further downregulated ERK phosphorylation, whereas all the colorectal cancer cell lines showed a rebound in phospho-ERK levels (Fig. 1C and D). We then examined the impact of AMG510 on the signaling network over time in NSCLC and colorectal cancer cell lines. At baseline, the colorectal cancer cell line C106 expressed lower levels of phosphorylated MEK and ERK with similar total protein relative to the NSCLC line NCIH358. Treatment with AMG510 decreased levels of active RAS-GTP, but the suppression was more pronounced in NCIH358 compared with C106. In C106, residual phospho-MEK and ERK were measurable already after 1 hour of treatment, whereas the NSCLC cell line (NCIH358) showed signs of rebound in phospho-MEK and phospho-ERK only at 72 hours after treatment (Supplementary Fig. S1A–S1C). Altogether, these data show that MAPK pathway inhibition upon AMG510 treatment is transient and less profound in colorectal cancer than lung models and suggest that this may be due to greater feedback suppression of MAPK signaling in colorectal cancer that is then released with KRAS^{G12C} inhibition.

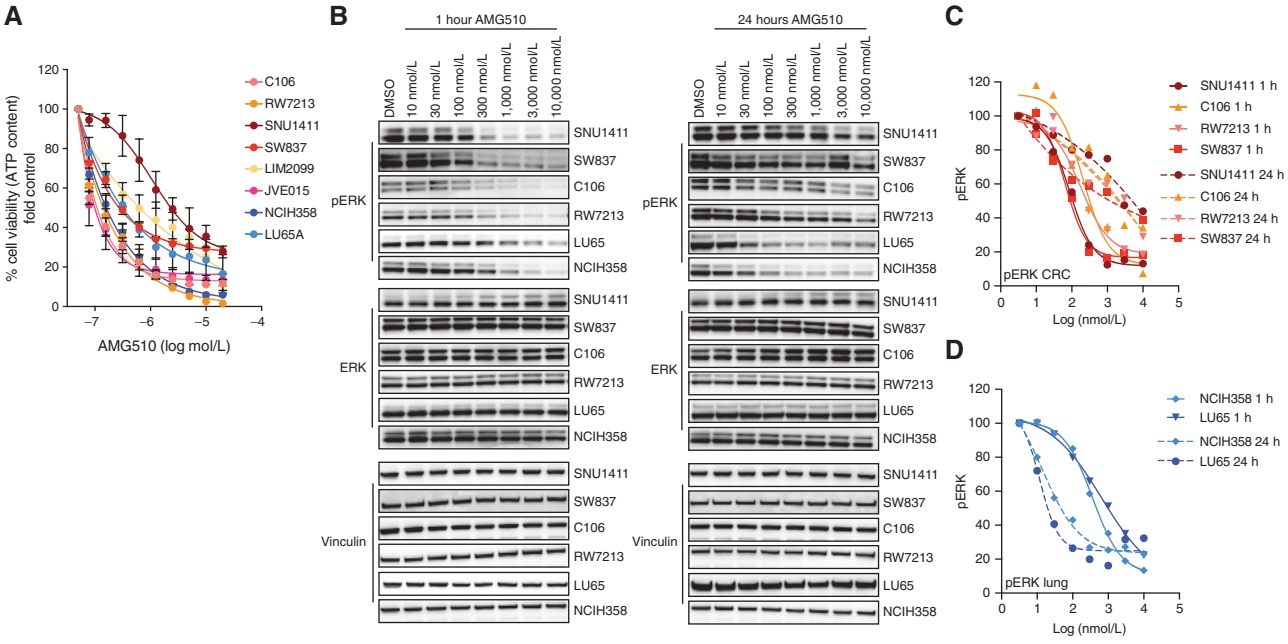

Figure 1. Response to KRAS^{G12C} inhibition in colorectal cancer (CRC) cell lines. **A,** Short-term proliferation assay of colorectal cancer cell lines (shades of red) and NSCLC cell lines (shades of blue). Cells were treated for 120 hours with increasing concentration of AMG510 and then ATP content was measured using CellTiter-Glo. Data represents the average and SD of at least three biological replicates. First data points of the curves represent the DMSO control. **B,** Western blot analysis of ERK activation upon AMG510 dose–response treatment after 1- and 24-hour treatment. Vinculin is used as loading control. **C,** Densitometry analysis of colorectal cancer cell lines in Western blot analysis in **B**. pERK values are normalized on both ERK and vinculin and on DMSO control. **D,** Densitometry analysis of NSCLC cell lines in Western blot analysis in **B**. pERK values are normalized on both ERK and vinculin and on DMSO control.

Colorectal Cancer Cells Bearing the KRAS^{G12C} Mutation Display High Basal RTK Activation

KRAS mutation acts downstream of RTK signaling and leads to constitutive ERK activation; in turn, high ERK levels feedback inhibit receptor signaling (19). KRAS-mutant proteins are thought to be constitutively active; therefore, it would be expected that *KRAS*-mutant tumors do not rely on RTK activation. To characterize the basal level of RTKs in patient tumors, we assembled a series of colorectal cancer and NSCLC clinical samples carrying the *KRAS*^{G12C} mutation. We analyzed eight colorectal cancer and five NSCLC patient specimens (Supplementary Table S1), all collected before any targeted therapy treatment, and evaluated the expression of 72 different proteins, including RTKs, using a selected reaction monitoring-mass spectrometry (SRM-MS) assay (see Methods). Detectable levels of EGFR, HER2, and MET were present in both lineages without clear differences, whereas HER3 expression was more prevalent in colorectal cancer patient samples (Fig. 2A). We did not detect ALK, ROS1, RET, FGFR, or AXL expression in any of the samples. Two patients with colorectal cancer and 2 patients with NSCLC later went on the phase I trial of AMG510 (Supplementary Table S1). Despite similar basal total RTK levels in the tumors from trial-enrolled patients, both NSCLC cases achieved clinical benefit, whereas both patients with colorectal cancer progressed upon AMG510 treatment. These data indicate that even in the presence of *KRAS*^{G12C} mutation, tumors often express upstream RTKs, predominantly consisting of HER family and MET receptors. However, the levels of total RTK expression do not appear to underlie lineage-specific differential response to KRAS^{G12C} inhibition between patients with colorectal cancer and patients with NSCLC.

Although we were able to detect total RTK expression in the clinical samples, we could not assess activated RTK levels or evaluate the functional consequences of detectable RTK expression in these tumors. To test this, we measured the levels of active RTKs in colorectal cancer and NSCLC cell lines using phospho-RTK arrays. The NSCLC cell line, NCIH358, had no detectable basal RTK activation and low levels of the phospho-EGFR and phospho-IGF1R could be detected only with signal enhancement through long exposure. In contrast, both colorectal cancer cell lines, C106 and RW7213, showed a number of detectable phosphorylated RTKs (Fig. 2B). Marked phospho-EGFR signal was present in both colorectal cancer models and was accompanied by detectable levels of other phosphorylated receptors. Coimmunoprecipitation assays using cetuximab as a capture antibody confirmed that EGFR is bound to the other HER receptors, MET and FGFR, suggesting heterodimerization processes (Supplementary Fig. S2A and S2B). Several Ephrin receptors (EphR) were also found activated in colorectal cancer cell lines. Interestingly, EphR activation has been reported as a mechanism of resistance to cetuximab in colorectal cancer and head and neck squamous cell carcinoma, suggesting that the cross-talk between these two classes of RTKs can potentially amplify EGFR signaling (20).

We next investigated the functional effect of the high levels of basal RTK activation in the colorectal cancer cell lines by evaluating the signaling consequences of EGF stimulation over time. At baseline, signaling downstream of RAS (phospho-AKT, phospho-MEK, and phospho-ERK) was lower in

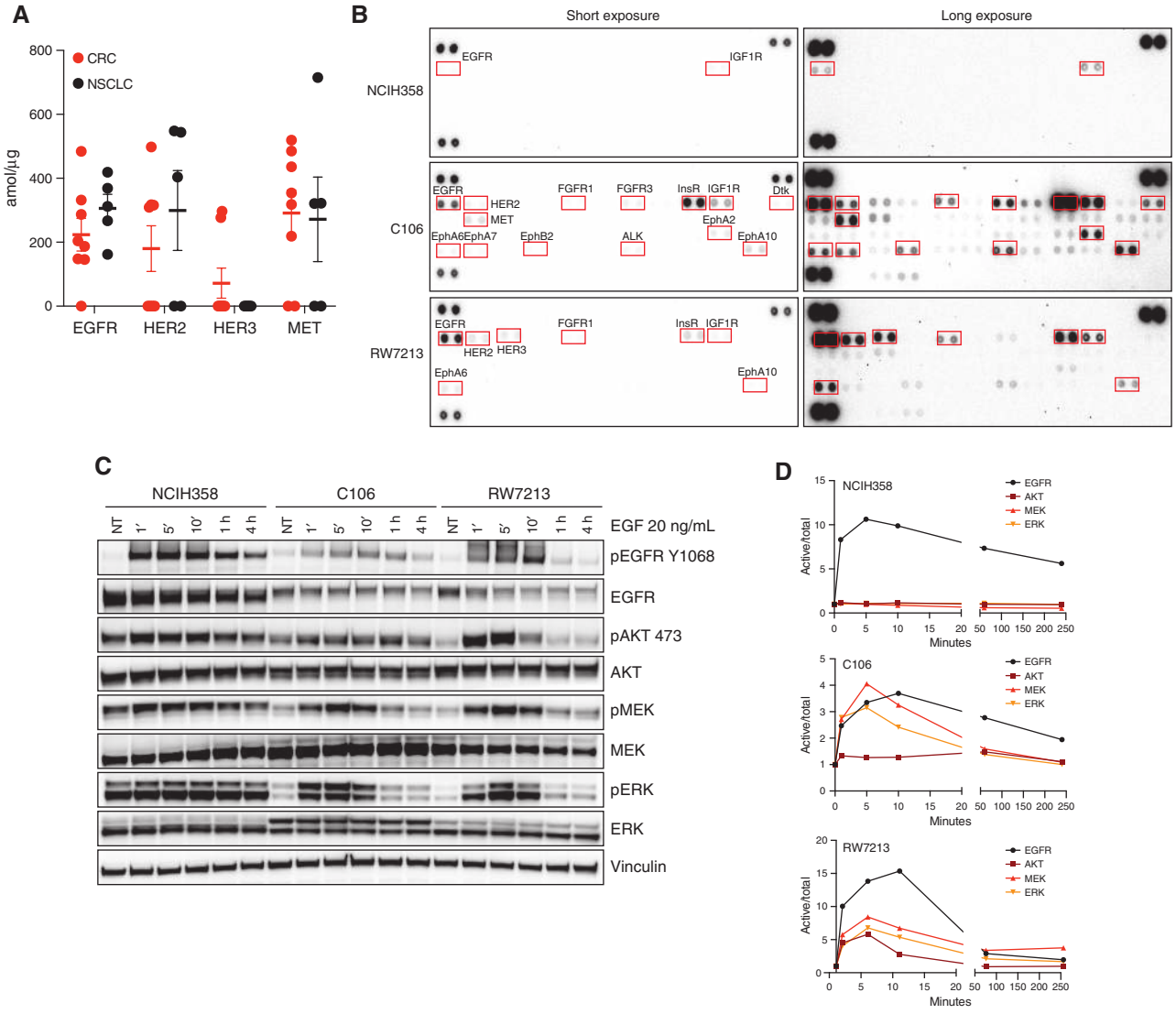

Figure 2. RTK component and responsiveness in colorectal cancer (CRC) cell lines. **A,** Mass spectrometry analysis of RTK in colorectal cancer and NSCLC patient-derived biopsies. **B,** Phospho-RTK array of NCIH358 (NSCLC), and C106 and RW7213 (colorectal cancer) cell lines. Cell were FBS starved for 24 hours and stimulated with 20% FBS for 10 minutes before harvesting. **C,** Western blot analysis of KRAS downstream effectors in NCIH358 (NSCLC), and C106 and RW7213 (colorectal cancer) cell lines upon time course EGF treatment. Vinculin is used as loading control. **D,** Densitometry analysis of pAKT, pMEK, and pERK of Western blot analysis in **C**. Phospho-proteins values are normalized on total proteins and vinculin and on not treated (NT) control.

the colon cancer cell lines compared with the NSCLC cell line, NCIH358. EGF treatment led to induction of phospho-EGFR in all cell models (Fig. 2C). However, activation of downstream effectors showed lineage-specific differences. The NSCLC cell line, NCIH358, did not show any modulation of AKT, MEK, or ERK phosphorylation upon EGF treatment, suggesting that KRAS^{G12C} does not get (further) activated by EGFR stimulation and can sustain downstream signaling without upstream inputs (Fig. 2C and D). In contrast, in the colorectal cancer cell lines, C106 and RW7213, downstream effectors followed the same kinetics of EGFR activation, showing that KRAS^{G12C} can be activated by upstream signaling components and that basal activation of RAS downstream effectors may be lower due to negative feedback loops (Fig. 2C and D). Altogether, these data indicate that even in the presence of the same KRAS-activating mutation, lineage-specific differences exist in the degree of RTK activation, contribution of upstream receptors to ERK activation (and thus rate of cycling of KRAS between the GTP- and GDP-bound forms), and feedback mechanisms that would be released from suppression by selective KRAS inhibitor–mediated ERK inhibition.

Cetuximab Sensitizes *KRAS*^{G12C} Colorectal Cancer Cell Lines to AMG510 and Concomitant EGFR and KRAS^{G12C} Blockade Reverts Secondary Resistance to Anti-EGFR Antibodies

On the basis of the high levels of basally active EGFR, the contribution of EGFR to KRAS^{G12C} signaling outputs, and the known relevance of EGFR signaling in colorectal cancer, we next evaluated whether KRAS^{G12C}–EGFR combined inhibition

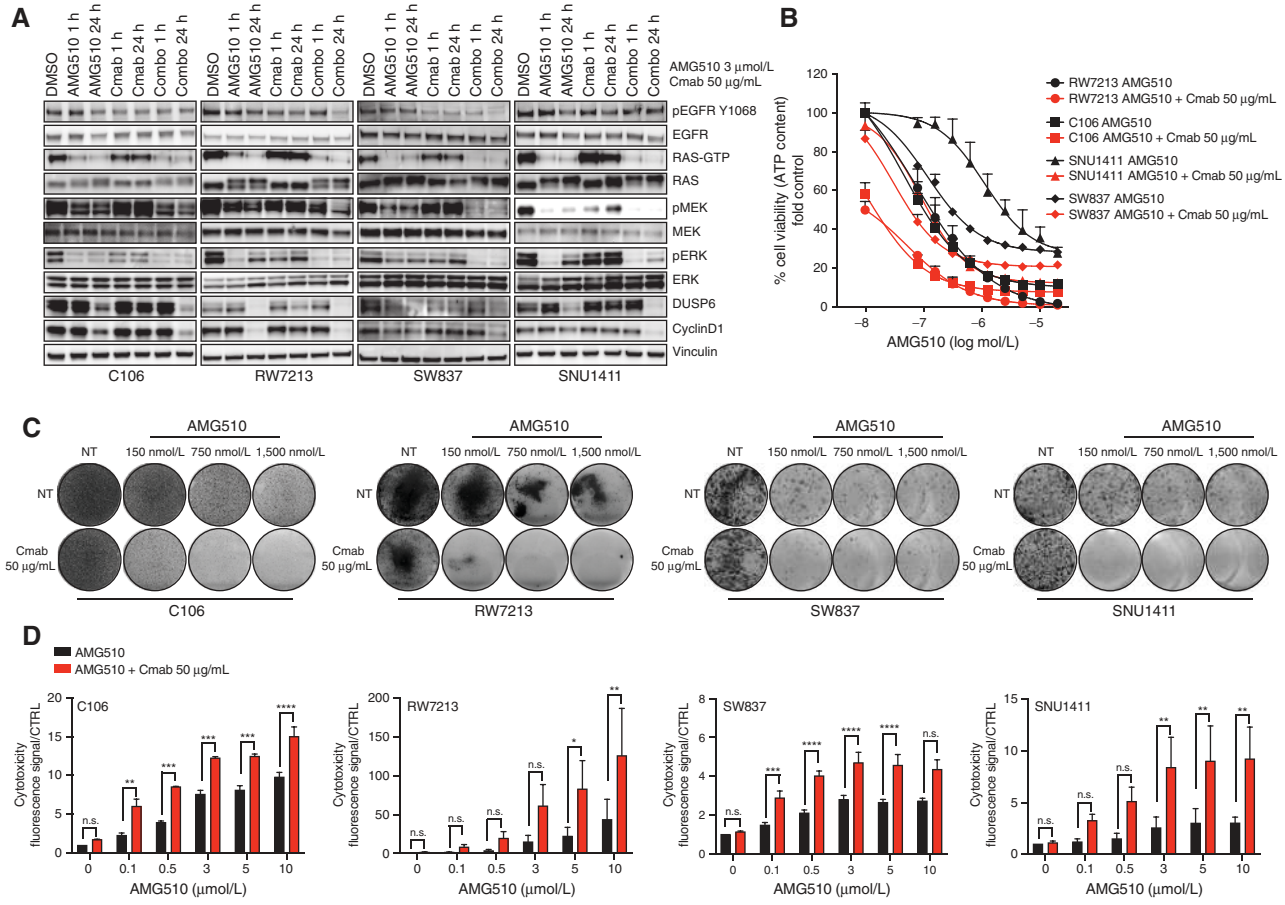

Figure 3. EGFR inhibition sensitizes colorectal cancer cell lines to AMG510. **A,** Western blot analysis of cetuximab (Cmab) plus AMG510 combinatorial (Combo) treatment time course in C106, RW7213, SNU1411, and SW837 colorectal cancer cell lines. RAS-GTP pulldown assay is included, and vinculin is used as loading control. **B,** Short-term proliferation assay of C106, RW7213, SNU1411, and SW837 treated with increasing concentration of AMG510 with or without 50 μg/mL cetuximab. First data points of the AMG510 single-agent curves represent the DMSO control. First data points of the combination curves represent the response to cetuximab alone. Cells were treated for 120 hours with increasing concentration of AMG510 and then ATP content was measured using CellTiter-Glo. Data represents the average and SD of three biological replicates. The AMG510 single-agent curves used in this graph are the same used in Fig. 1A. **C,** Long-term drug screening proliferation assay of C106, RW7213, SNU1411, and SW837 treated with increasing concentration of AMG510 with or without 50 μg/mL cetuximab. Cetuximab-only–treated cells are shown in the first bottom circles. Cells were treated for 9–13 days according to the time when untreated controls reached confluence. **D,** CellTox assay of C106, RW7213, SNU1411, and SW837 treated with increasing concentration of AMG510 with or without 50 μg/mL cetuximab. Cetuximab-only–treated cells are shown as the first red bar at 0 μmol/L AMG510. Cells were treated for 120 hours. Data represents the average and SD of three biological replicates with the exception of the C106 graph that represents a biological duplicate. Statistical significance was calculated using one-way ANOVA with Bonferroni correction. *, $P < 0.05$; **, $P < 0.01$; ***, $P < 0.001$; ****, $P < 0.0001$; n.s., not significant. (*continued on next page*)

could effectively suppress signaling and growth in the colorectal cancer models. Biochemical analysis and densitometric quantitation of phosphoprotein levels showed that concomitant KRAS^{G12C} and EGFR inhibition, with AMG510 and the anti-EGFR antibody cetuximab, respectively, led to sustained inhibition of phospho-MEK and phospho-ERK, as well as the ERK downstream targets DUSP6 and CyclinD1, indicating inhibition of ERK output (Fig. 3A; Supplementary Fig. S3A and S3B). Colorectal cancer cell lines were also tested in short-term proliferation assays. ATP content measurement showed that concurrent treatment with the EGFR inhibitor cetuximab synergized with AMG510 in all the cell lines tested (Fig. 3B; Supplementary Fig. S4A). Growth suppression was durable, as similar effects were also seen in long-term proliferation assays stained with crystal violet (Fig. 3C).

We next sought to determine whether combined KRAS and EGFR inhibition could lead to cell death together with cell proliferation arrest. We found that the combination treatment induced a pronounced cytotoxic effect, as measured by detection of DNA of cells with impaired membrane integrity, in all the models tested and across dose levels of AMG510 (Fig. 3D). These data indicate that combined KRAS^{G12C} and EGFR inhibition leads to increase cell death rate.

To further assess the role of EGFR signaling in AMG510 resistance, we used the *KRAS* wild-type, cetuximab-sensitive colorectal cancer cell line LIM1215 to generate isogenic models carrying the *KRAS*^{G12C} allele using an AAV-mediated knock-in approach (21). As expected, all *KRAS*^{G12C}-mutant clones (KI#1, KI#2, and KI#3) showed resistance to cetuximab as a single agent (Fig. 3E). *KRAS*^{G12C}-mutant clones were more sensitive to

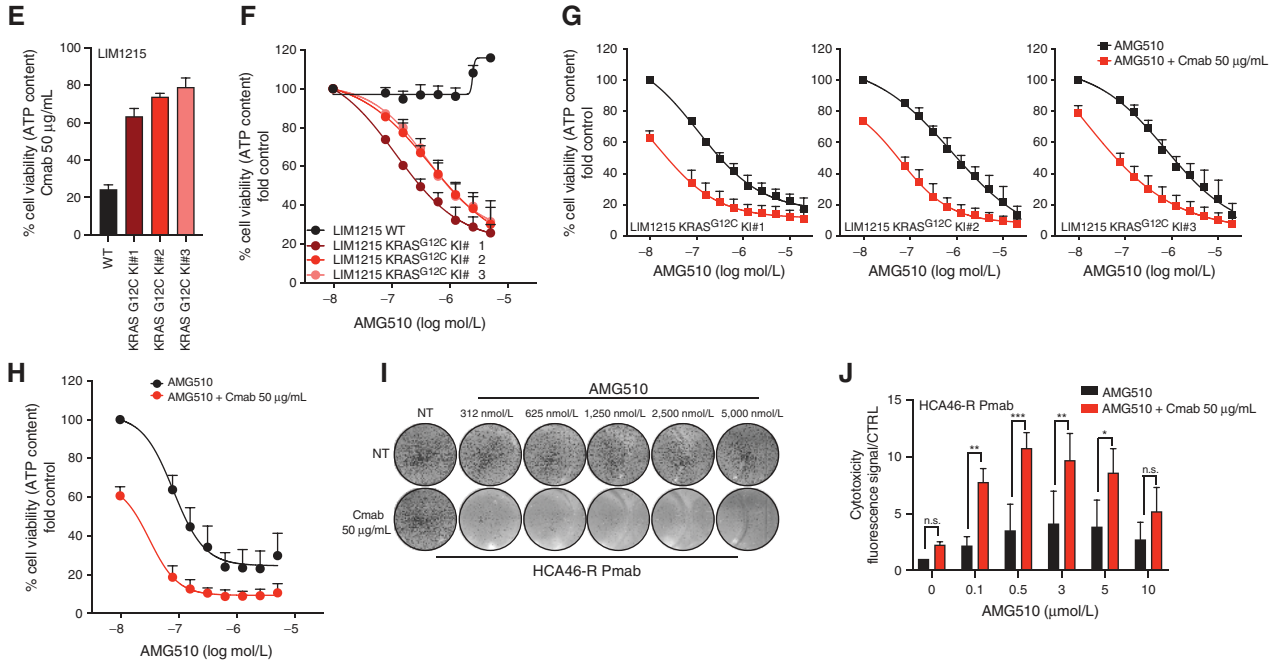

Figure 3. ***(Continued)*** **E,** LIM1215 KRAS^{G12C} knock-in (KI) clones response to cetuximab; these data correspond to the first data points of the combination arms in **G**. LIM1215 parental cells were included as control. **F,** LIM1215 KRAS^{G12C} KI clones' response to AMG510 in short-term proliferation assay. Cells were treated for 120 hours with increasing concentrations of AMG510, and then ATP content was measured using CellTiter-Glo. Data represents the average and SD of three biological replicates. First data points of the AMG510 single-agent curves represent the DMSO control. **G,** LIM1215 KRAS^{G12C} KI clones' response to AMG510 + cetuximab in short-term proliferation assay. First data points of the AMG510 single-agent curves represent the DMSO control. First data points of the combination curves represent the response to cetuximab alone. Cells were treated for 120 hours with increasing concentration of AMG510 and then ATP content was measured using CellTiter-Glo. Data represents the average and SD of three biological replicates. The AMG510 single-agent curves are the same as in **F**. **H,** HCA46-R panitumumab (Pmab) cell line response to AMG510 + cetuximab in short-term proliferation assay. First data point of the AMG510 single-agent curve represents the DMSO control. First data point of the combination curve represents the response to cetuximab alone. Cells were treated for 120 hours with increasing concentration of AMG510, and then ATP content was measured using CellTiter-Glo. Data represents the average and SD of three biological replicates. **I,** Long-term drug screening proliferation assay of HCA46-R Pmab treated with increasing concentration of AMG510 with or without 50 µg/mL cetuximab. Cetuximab-only–treated cells are shown in the first bottom circles. **J,** CellTox assay of HCA46-R Pmab treated with increasing concentration of AMG510 with or without 50 µg/mL cetuximab. Cetuximab-only–treated cells are shown as the first red bar at 0 µmol/L AMG510. Data represents the average and SD of three biological replicates. Statistical significance was calculated using one-way ANOVA with Bonferroni correction. *, $P < 0.05$; **, $P < 0.01$; ***, $P < 0.001$; ****, $P < 0.0001$; n.s., not significant.

AMG510 than their wild-type counterpart (Fig. 3F). The addition of cetuximab in combination with KRAS^{G12C} inhibition was synergistic compared with the single agent alone (Fig. 3G; Supplementary Fig. S4B). These results provide further support that EGFR and KRAS^{G12C} should be concomitantly inhibited to overcome resistance to KRAS^{G12C} inhibition in colorectal cancer.

We and others previously reported that acquired *KRAS* mutations are responsible for secondary resistance to anti-EGFR therapies in colorectal cancer (22, 23). We reasoned that KRAS inhibitors could have clinical applications in patients who develop *KRAS* mutations at relapse after EGFR blockade. To directly test this possibility, we used a colorectal cancer cell line (HCA46-R Pmab), in which prolonged treatment with panitumumab led to the emergence of a *KRAS*^{G12C} allele (24). We examined whether AMG510 could be effective in this setting. Although single-agent AMG510 treatment was partially effective, its combination with cetuximab induced both cell proliferation arrest and cell death (Fig. 3H–J; Supplementary Fig. S4C). These data suggest that also in the secondary resistance setting, colorectal cancer cells could retain upstream signaling dependency.

Colorectal Cancer Patient-Derived Models Are Sensitive to Combinatorial EGFR–KRAS^{G12C} Inhibition

To test whether and to what extent these findings were applicable to clinically relevant models, we collected biopsies and exploited established models from patients with colorectal cancer generated in our institutions (Supplementary Tables S2 and S3).

Taking advantage of our molecularly and therapeutically annotated colorectal cancer patient–derived biobank (25–27), in a cohort of more than 100 patient-derived organoids (PDO), we selected three different *KRAS*^{G12C}-mutant PDOs and one *KRAS*^{G12D}-mutant PDO (as negative control) and tested the effects of single agents AMG510 and cetuximab and their combination.

In the *KRAS*^{G12C} PDOs, single-agent AMG510 or cetuximab did not inhibit or poorly inhibited growth, whereas the combination suppressed proliferation with high synergy scores (Fig. 4A–C).

In parallel, we generated patient-derived xenografts (PDX) from 2 patients with *KRAS*^{G12C}-mutant colorectal cancer and tested AMG510 and cetuximab as single agents and in combination *in vivo*. Both models exhibited slow but persistent growth when mice

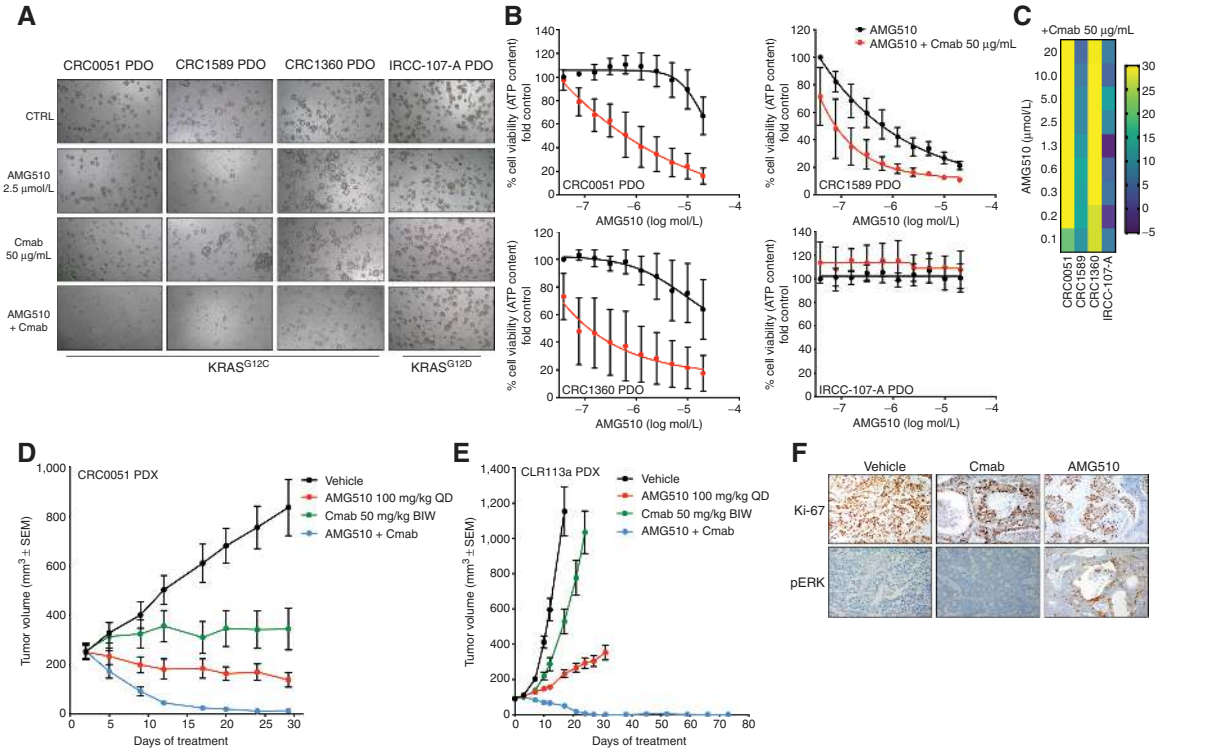

Figure 4. AMG510 + cetuximab combination is effective in *KRAS*^{G12C}-mutant patient-derived models. **A,** Brightfield microscopy images of PDO treated with vehicle, AMG510, cetuximab, and the combination 7 days after treatment. **B,** ATP content quantification with CellTiter-Glo assay. First data points of the AMG510 single-agent curves represent the DMSO control. First data points of the combination curve represent the response to cetuximab alone. **C,** Synergy score. Heat map of excess over the Bliss (Bliss score) for AMG510–cetuximab (Cmab) combination. **D,** CRC0051 KRAS^{G12C}-mutant colorectal cancer (CRC) PDXs were treated with vehicle alone, AMG510 100 mg/kg orally once a day (QD), cetuximab 50 mg/kg intraperitoneally twice a week (BIW), or the combination of the two drugs at the same doses. Error bars represent SEM (minimum 5 animals per group). **E,** CLR113a KRAS^{G12C}-mutant colorectal cancer PDXs were treated with vehicle alone, AMG510 100 mg/kg orally once a day, cetuximab 50 mg/kg intraperitoneally twice a week, or the combination of the two drugs at the same doses. Error bars represent SEM (5 animals per group). **F,** Ki-67 and phospho-ERK IHC staining of the CLR113a PDX samples collected at the end of treatment from vehicle-, cetuximab-, and AMG510-treated arms. Ki-67 IHC intensity of 97% with no necrosis in vehicle-treated mice, 92% with necrosis in cetuximab-treated mice, and 83% with necrosis in AMG510-treated mice.

were treated with either cetuximab or AMG510 single-agent treatment. Combination treatment induced massive or even complete tumor shrinkage in the treated animals (Fig. 4D and E). No tumor was visible after 10 weeks of treatment and no samples could be collected at the end of the PDX experiment (Fig. 4E). Interestingly, IHC staining for the proliferation marker Ki-67 was highly positive in tumor samples derived from vehicle-, cetuximab-, and AMG510-treated arms (Ki-67 IHC intensity of 97% with no necrosis in vehicle-treated mice, 92% with necrosis in cetuximab-treated mice, and 83% with necrosis in AMG510-treated mice), but strong phospho-ERK staining was observed only in the AMG510-treated samples, suggesting that strong MAPK pathway rebound occurs in patient-derived samples as well (Fig. 4F).

DISCUSSION

Recent clinical data have shown promising activity of agents targeting mutant (G12C) KRAS, a heretofore undruggable target. These trials, however, show substantial differences in the response rate between patients with NSCLC and patients with colorectal cancer (14, 15).

We found that KRAS^{G12C} inhibitors produce less profound and more transient inhibition of KRAS downstream signaling in colorectal cancer versus NSCLC models. Our data indicate that, despite harboring the same mutation, there are intrinsic differences in signaling between colorectal cancer and NSCLC. Our data suggest that in colorectal cancer the combination of (i) signaling rebound upon KRAS^{G12C} inhibition, (ii) the higher extent of RTK activation, and (iii) the stronger response to EGFR direct stimulation can be used to define the intrinsic dependency of bowel tumors on the EGFR–MAPK pathway. These results, together with the emerging clinical experience with single-agent KRAS^{G12C} inhibitors, indicate that combinatorial treatment is necessary to effectively treat *KRAS*^{G12C}-mutant colorectal cancer.

This is, to our knowledge, the first study aimed at specifically characterizing the effects of KRAS^{G12C} inhibition in colorectal cancer. Indeed, the main goal of this work was to understand and exploit colorectal cancer lineage–specific features to develop more effective pharmacologic strategies.

It is known that RTK inhibition in NSCLC preclinical models can potentiate KRAS^{G12C} covalent inhibitors by slowing down exchange factors favoring a GDP-bound status of KRAS (8). However, this combinatorial strategy is considered only marginal in this setting, as other combinatorial partners including PI3K, mTOR, and Aurora kinase inhibitors have been shown to

have higher efficacy than EGFR inhibition in combination with KRAS^{G12C} inhibition in lung cancer (10, 12, 13).

We found that expression of EGFR and its dimerization partners is common in *KRAS*^{G12C} colorectal cancer and NSCLC clinical samples. Basal EGFR expression, as measured by IHC or mass spectrometry (28, 29), has not been associated with EGFR inhibitor sensitivity in colorectal cancer, and indeed we find no clear difference between receptor expression levels by lineage or in the subset of patients with colorectal cancer and NSCLC treated with AMG510. In cell line models, however, we are able to assess activated RTK levels, and we find that the degree of this dependency on RTK signaling across *KRAS*^{G12C}-mutant tumors can be very different. Specifically, we show that *KRAS*^{G12C}-mutant colorectal cancer cell lines still retain their dependency on EGFR for downstream signaling.

The clinical and signaling effects of AMG510 in colorectal cancer are reminiscent of the clinical experience in *BRAF*^{V600E} colorectal cancer, where the concomitant inhibition of upstream signaling reactivation results in improved clinical efficacy (30), which has led to the recent FDA approval of the BRAF inhibitor encorafenib in combination with cetuximab (BEACON colorectal cancer; NCT02928224).

Clinical trial results have shown limited efficacy of KRAS^{G12C} covalent inhibitors in colorectal cancer; only 1 patient with colorectal cancer treated with MRTX849 had a 47% tumor reduction by RECIST criteria (15). Our results show that in colorectal cancer cell models and in PDX, treatment with AMG510 single agent induces strong reactivation of MAPK pathway. These data indicate that even in the best scenario, up-front combination treatment is the best option for patients with *KRAS*^{G12C}-mutant colorectal cancer, as this approach would enhance the efficacy of KRAS^{G12C} inhibitors and would also limit the emergence of acquired resistance.

We showed that KRAS^{G12C}-mutant colorectal cancer still retains EGFR–MAPK dependency, as demonstrated by the signaling rebound upon KRAS^{G12C} inhibition, the more pronounced activation of RTKs, and the high response to EGFR direct stimulation. We can speculate that other *KRAS*-mutant alleles in colorectal cancer could also retain these characteristics, suggesting that other *KRAS*-mutant colorectal cancers could also potentially benefit from EGFR-based combinations. Therefore, direct or indirect KRAS blockade–based combinations could be considered as an option in these specific settings.

Combined inhibition of KRAS^{G12C} with SHP2, a phosphatase that serves as a common mediator of RTK signaling to RAS (31), has been proposed as another combination to overcome the feedback reactivation in KRAS^{G12C} tumors (32).

Available clinical data with SHP2 inhibitors is currently limited, and it is not yet known whether these inhibitors can be administered to patients in sufficient doses to effectively inhibit RTK signaling. Furthermore, preclinical models suggest growth suppression but not complete tumor regression with SHP2 and KRAS^{G12C} inhibitors, in contrast to the complete, durable tumor inhibition achieved in a PDX treated with EGFR and KRAS^{G12C} inhibitors.

Because RTK signaling in colorectal cancer is mostly dominated by wild-type EGFR, we propose to combine KRAS^{G12C} inhibitors with anti-EGFR mAbs to block receptor signaling rather than inhibiting EGFR kinase activity. Moreover, the differential activity of EGFR inhibitors in colorectal cancer versus NSCLC further indicates signaling differences in these two lineages (33). The anti-EGFR antibodies cetuximab and panitumumab are approved for the treatment of RAS/RAF wild-type colorectal cancer (34, 35), whereas EGFR tyrosine kinase inhibitors (TKI) are approved for the treatment of *EGFR*-mutant lung cancer (36). EGFR-targeting TKI have not been effective in colorectal cancer (37), probably because *EGFR* genetic alterations are rare in colorectal cancer and these drugs are more efficient in the *EGFR*-mutant setting. As release of wild-type receptor signaling from feedback inhibition is thought to mediate adaptive resistance to targeted therapies, the role of wild-type EGFR in activating signaling in colorectal cancer could render colorectal cancers more sensitive to this feedback release than NSCLC.

Taken together, our results demonstrate that biochemical characterization of response to KRAS^{G12C} inhibitors in colorectal cancer provides a mechanistic explanation for their limited activity in the clinic and, at the same time, provides a strong rationale to combine EGFR blockade with these agents in patients with colorectal cancer.

METHODS

Cell Lines and Compounds

The cell lines NCIH358, LU65, SNU1411, JVE015, LIM2099, LIM1215, LIM1215 KRAS G12C KI, and RW7213 were cultured in RPMI (Lonza). The C106 cell line was cultured in Iscove's Modified Medium (Lonza). The SW837 cell line was cultured in DMEM/F12 (Lonza). The HCA46-R Pmab cell line was cultured in DMEM (Lonza). Each medium was supplemented with 10% FBS, 2 mmol/L L-glutamine, 100 U/mL penicillin, and 100 mg/mL streptomycin. The SW837 and NCIH358 cell lines were purchased from the ATCC; the C106 and HCA46 cells were purchased from the European Collection of Animal Cell Cultures; the SNU1411 cells were purchased from KCLB; the LU65 cells were purchased from AcceGen Biotech; the LIM2099 cells were provided by Dr. F. Walker (The Walter & Eliza Hall Institute of Medical Research, Ludwig Institute for Cancer Research, Melbourne-Parkville Branch, Parkville, Victoria, Australia). LIM1215 cells were kindly provided by Dr. Whitehead (Vanderbilt University, Nashville, TN); JVE015 cells were provided by Prof. Tom Van Wezel (Leiden University Medical Center, Leiden, the Netherlands); and RW7213 cells were provided by Dr. Diego Arango (Institute of Biomedical Research of Lleida, Lleida, Spain).

All the cell lines were determined to be *Mycoplasma* free using the Venor GeM Classic Kit (Minerva Biolabs) and tested by short tandem repeats profiling at 10 different loci.

AMG510 was purchased from ChemGood (C-1499) and cetuximab was either gifted from Merck Serono under an academic material transfer agreement or purchased from the pharmacy at Memorial Sloan Kettering Cancer Center (New York, NY).

PDOs

All the procedures performed with patient specimens were conducted under the approval of the local ethical committee of the institutions, after the written informed consent of the patients. CRC1589, CRC1360, and CRC0051 PDOs were derived from PDXs established from three distinct patients with KRAS^{G12C} colorectal cancer, whereas IRCC107A PDO was established directly from tissue biopsy obtained at the time of surgery. To generate PDX-derived organoids, PDX samples were first dissociated mechanically with gentle MACS Dissociator (Miltenyi Biotec) and then underwent enzymatic digestion of extracellular matrix using Human Tumor Dissociation Kit (Miltenyi Biotec). The derived single-cell suspension was centrifuged at 400 × *g* for 5 minutes and then resuspended in the organoids' basal medium. Cell suspension was

filtered with 70-μm cell strainer to avoid cell cluster formation. The flow-through was centrifuged and the pellet was resuspended in Matrigel (Corning) and dispensed as 100 μL droplet in the center of 37°C prewarmed 12-well plate. After an incubation of 15 minutes at 37°C for Matrigel solidification, organoids were added with ENAS medium and incubated at 5% CO_2 and 37°C. ENAS medium was refreshed twice per week.

To generate PDOs directly from patient tissue biopsy, tumor tissue was first smashed into small pieces and incubated in PBS with collagenase A (0.5 mg/mL; Roche), hyaluronidase (20 mg/mL; Sigma), and 10 mmol/L ROCK inhibitor for 30 minutes at 37°C with shaking. After incubation, 5% FBS was added and the mixture was centrifuged at 400 × *g* for 5 minutes. The pellet was washed three times in PBS to remove debris and collagenase. At the end of the washing phase, the pellet was resuspended in Matrigel (Corning) and 50 μL of organoids–Matrigel suspension was dispensed into the center of each well of a 37°C prewarmed 24-well plate. Different densities of tumor cells were plated and left to solidify for 10–30 minutes at 37°C before ENAS medium was added and the cells were incubated at 37°C, 5% CO_2. Fresh medium was replaced every 2–3 days. Outgrowing organoids were passaged every 10–15 days after mechanical and enzymatic disruption. Organoid drug treatment was performed in each organoid-specific culture medium at 37°C and 5% CO_2.

The organoid basal medium was composed of Advanced DMEM/F12 Medium (Thermo Fisher Scientific) containing 100 U/mL penicillin, 100 μg/mL streptomycin, 2 mmol/L Glutamax (Gibco), 10 mmol/L Hepes, and 50 μg/mL Primocin (Invitrogen). ENAS medium was prepared by adding 1× B27 supplement (Invitrogen), 1× N2 supplement (Invitrogen), 1.25 mmol/L N-acetyl-cysteine (Sigma Aldrich), 10 mmol/L Nicotinamide (Sigma Aldrich), 10 nmol/L Gastrin (Sigma), 50 ng/mL recombinant mouse EGF (Life Technologies), 100 ng/mL Noggin (PeproTech), 500 nmol/L TGFb type I receptor inhibitor A83-01 (Tocris), and 10 μmol/L p38 MAPK inhibitor SB202190 (Sigma Aldrich) to the organoid basal medium.

Antibodies and Western Blotting

After seeding and drug treatments, cells were washed with cold PBS and lysed in RIPA buffer (Pierce #89901) plus phosphatase and protease inhibitors (Thermo Fisher Scientific #1861277 and #1861278). Lysates were cleared by centrifugation at 14,000 rpm at 4°C and quantified using BCA Method (Pierce #23224).

Samples were prepared using LDS+Reducing Agent Novex Buffers (Invitrogen #NP0008 and #NP0009). Ten to 20 μg of lysates were loaded and run on NuPageTM 4%–12% Bis-Tris Gels (Thermo Fisher Scientific #NP0321BOX) followed by transfer to nitrocellulose membranes (Bio-Rad #1620233). Membranes were incubated overnight with the indicated antibodies, washed, and incubated again for 45 minutes with anti-rabbit or anti-mouse secondary antibodies. Detection was performed using Immobilion Western (Millipore #WBKLS0500).

Primary antibodies were obtained from Cell Signaling Technology and were used at a concentration of 1:1,000: pAKT S473 (#9271), pMEK1/2 S217/221 (#9154), p-p44/42 MAPK T202/204 (#9101), MEK1/2 (#9122), ERK1/2 (#9102), AKT (#9272), EGFR (#2232S), phospho-EGFR Tyr1068 (#3777S), and Vinculin (#13901S). DUSP6 antibody was purchased from Abcam (#ab54940) and used at 1:500 dilution. CyclinD1 antibody was purchased from Santa Cruz Biotechnology (#sc-718) and used at 1:1,000 dilution. Densitometry analyses were performed using ImageJ software.

EGFR Immunoprecipitation

For immunoprecipitation assays, cells were seeded and starved for 24 hours and then stimulated with 20% FBS for 10 minutes. Cells were then washed in cold PBS and lysed using NP-40 buffer (150 mmol/L NaCl, 10 mmol/L Tris pH 8, 1% NP-40, and 10% glycerol). Proteins (20 μg) were used as total lysates. Protein lysates (1,500 μg) were incubated rotating at 4°C for 1.5 hours in the presence of 10 μg/mL cetuximab, Agarose protein G beads (Invitrogen #15920-010). Beads were centrifuged at 3,000 rpm for 1 minute and supernatant was removed. Similarly, beads were washed three times using NP-40 buffer and once using nuclease-free sterile water. Finally, immunoprecipitates were eluted using 1× sample buffer (NuPAGE LDS Sample Buffer, Thermo Fisher Scientific #NP0008 and NuPAGE Sample Reducing Agent, Thermo Fisher Scientific #NP0009) at 95°C for 5 minutes.

RAS-GTP Pulldown Assay

RAS-GTP pulldown assay was performed according to the manufacturer's protocol (Thermo Fisher Scientific #16117). Briefly, 500 μg of lysates were loaded into columns together with agarose beads and RAS-RBD bait and incubated for 1 hour at 4°C. After the incubation, beads were washed three times and resuspended in LDS+Reducing Agent Novex Buffers (Invitrogen #NP0008 and #NP0009). A fraction of lysates was used to measure total RAS amount. Pulldown and total lysates were subjected to Western blotting procedure as described above. The kit provided primary antibody against pan-RAS.

Phospho-RTK Array

Human Phospho-RTK Arrays (R&D Systems, ARY001B) were used to detect activated RTKs according to the manufacturer's instructions. Cells were washed with cold PBS and lysed using the provided lysis buffer plus phosphatase and protease inhibitors. Lysates (200 μg) were incubated on membranes overnight. Membranes were subsequently washed and exposed to chemiluminescent reagent.

Mass Spectrometry

SRM-MS of 72 biomarkers of the tissue sections from formalin-fixed, paraffin-embedded (FFPE) blocks was conducted as described previously (38, 39). Briefly, two tissue sections (10 μm each) from FFPE blocks were placed on DIRECTOR slides, deparaffinized, and stained with hematoxylin. Tumor areas were marked by a board-certified pathologist, and then were microdissected and solubilized to tryptic fragments as per the manufacturer's instructions (Expression Pathology). Protein concentration of the tryptic peptides was calculated using microBCA. Stable heavy isotope-labeled internal standard peptides for 72 biomarkers were added to the solution and injected into the mass spectrometer (TSQ Quantiva, Thermo Fisher Scientific). On-column injection resulted in 5 fmol of isotopically labeled internal standard peptide and 1 μg of total tumor protein. Data analysis of the 72 biomarkers was conducted using Pinnacle Software (Optys Tech). All patients whose tumors were analyzed signed written informed consent for molecular profiling of their tumors (IRB 12-245) and approval was obtained for the mass spectrometry assay.

Drug Proliferation Assays

For short-term proliferation assays, 2,000 cells were seeded in 96-well culture plates in medium containing 10% FBS. After 24 hours, serial dilutions of AMG510 (alone or in combination with cetuximab) were added to cells in 10% FBS medium (ratio 1:1). Cell viability was determined at day 5 after the start of the treatment by measuring ATP content using CellTiter-Glo Luminescent Cell Viability Assay (Promega). DMSO only–treated cells were used as control. Excess over the Bliss (Bliss score) was calculated using effect of the combination (observed) versus what was predicted/expected on the basis of the effect of each single agent expressed as percentage. Negative values or values close to zero show no/very little synergy. Higher percentages indicate higher synergy.

For long-term proliferation assays, cells were seeded (5,000 cells per well for SNU1411, SW837, and HCA46R, and 80,000 cells per well for RW7213) in 24-well plates or in 6-well plates (C106 80,000 cells per well) in 10% FBS medium. The following day, plates were treated with different concentrations of drugs as indicated. Cells were fixed with 4% paraformaldehyde and stained with 10% crystal violet in a Methanol/Water Solution (Sigma Aldrich) 9–13 days after

the start of treatment, according to the confluence reached by the untreated control. Every 7 days, media and drug were refreshed. In all the experiments, plates were incubated at 37°C in 5% CO_2.

Short-term assays were performed at least three times. All long-term assays were performed independently at least three times for HCA-46R, SW837, and SNU114, and two times for C106 and RW7213. Analyses and graphs were performed with GraphPad Prism Software using the function log (inhibitor) versus response-variable slope (four parameters).

Drug Cytotoxicity Assay

For short-term cytotoxicity assay, 2,000 cell/well were seeded in 96-well plates and treated after 24 hours with AMG510 alone or in combination with cetuximab as indicated. After 5 days from the start of treatment, cell cytotoxicity was determined measuring the fluorescence of dead cells using CellTox Green Cytotoxicity Assay (Promega), according to the kit's instructions. The CellTox green results were normalized to results of CellTiter-Glo Luminescent Cell Viability assay conducted on the same plates. In all the experiments, plates were incubated at 37°C in 5% CO_2. All assays were performed independently at least three times.

In Vivo *Studies*

The CLR113 PDX was derived from a liver metastasis under written consent. Tumor tissue was transplanted orthotopically into NSG mice to establish the PDX (institutional review board protocols 06-107 and 14-091). Once a tumor became visible in the first mouse, it was transplanted and expanded to other animals. Tumor tissue was implanted subcutaneously in the flank of 4- to 6-week-old NSG female mice, and treatment of the mice began when tumors reached approximately 100 mm^3 in size. Mice were randomized ($n = 5$ mice per group) to receive drug treatments or vehicle as control. Studies were performed in compliance with institutional guidelines under an Institutional Animal Care and Use Committee (IACUC)–approved protocol. The animals were immediately euthanized as soon as the tumors reached the IACUC set limitations.

The CRC0051 PDX was derived from a colorectal cancer patient metastasis, under written consent. Patient tissue was transplanted into NOD/SCID mice to establish PDX and then transplanted and expanded to other animals. Tumor was implanted subcutaneously in the flank of 11- to 13-week-old NOD/SCID mice, and treatment of the mice began when tumor reached approximately 250 mm^3. Mice were randomized ($n = 7$ per arm) and received drug treatment or vehicle control.

AMG510 was given 100 mg/kg daily by gavage. Cetuximab was administered 50 mg/kg twice a week, by intraperitoneal injections.

The entire experiment was performed in compliance with institutional guidelines of the Ethical committee of Candiolo Cancer Institute (Candiolo, Torino, Italy) and according to the Italian Ministry of Health–approved protocol. The animals were sacrificed on the basis of the rules defined in the approved protocol.

Disclosure of Potential Conflicts of Interest

R. Yaeger is a consultant at Array BioPharma, reports receiving commercial research grants from Array BioPharma, Boehringer Ingelheim, and Novartis, and has an advisory board relationship with Array BioPharma. Y.R. Murciano-Goroff has received remuneration from AstraZeneca. N. Valeri has received speakers bureau honoraria from Bayer, Eli Lilly, Pfizer, and Merck. S. Thyparambil is a senior director R&D at mProbe. S. Siena is an advisory board member at Amgen, Bayer, BMS, CheckMab, Clovis, Daiichi-Sankyo, Merck, Roche-Genetech, and Seattle Genetics. L. Trusolino reports receiving commercial research grants from Symphogen, Servier, Pfizer, Merus, and Menarini, and has received speakers bureau honoraria from Eli Lilly, AstraZeneca, and Merck KGaA. B.T. Li is a consultant/advisor at Roche/Genentech, Biosceptre International, Thermo Fisher Scientific, Mersana Therapeutics, Hengrui Therapeutics, and Guardant Health, reports receiving commercial research grants from Roche/Genentech, Daiichi Sankyo, Amgen, Lilly, Hengrui Therapeutics, Illumina, Guardant Health, BioMedValley Discoveries, AstraZeneca, GRAIL, and MORE Health, and has ownership interest in two institutional patents at Memorial Sloan Kettering Cancer Center (US62/685,057, US62/514,661). N. Rosen is a SAB member at Beigene, MAPCure, AstraZeneca, Tarveda, Ribon, Chugai, and Zai Labs, is a consultant at Boehringer Ingelheim, reports receiving commercial research grants from Chugai and Boehringer Ingelheim, and has ownership interest (including patents) in Kura, Beigene, Zai Labs, Fortress, and Ribon. A. Bardelli reports receiving a commercial research grant from Neophore, has ownership interest (including patents) in Neophore, and has advisory board relationships with Horizon Discovery, Neophore, and Biocartis. S. Misale is a consultant at Boehringer-Ingelheim. No potential conflicts of interest were disclosed by the other authors.

Authors' Contributions

Conception and design: V. Amodio, R. Yaeger, N. Rosen, A. Bardelli, S. Misale

Development of methodology: V. Amodio, R. Yaeger, P. Arcella, M. Pinnelli, H.-Y. Zhao, L. Trusolino, F. Di Nicolantonio, S. Misale

Acquisition of data (provided animals, acquired and managed patients, provided facilities, etc.): V. Amodio, R. Yaeger, P. Arcella, S. Lamba, S. Arena, M. Montone, B. Mussolin, Y. Bian, M. Pinnelli, Y.R. Murciano-Goroff, E. Vakiani, N. Valeri, W.-L. Liao, A. Bhalkikar, S. Thyparambil, H.-Y. Zhao, E. de Stanchina, S. Siena, A. Bertotti, L. Trusolino, B.T. Li, F. Di Nicolantonio, S. Misale

Analysis and interpretation of data (e.g., statistical analysis, biostatistics, computational analysis): V. Amodio, R. Yaeger, P. Arcella, S. Arena, Y.R. Murciano-Goroff, E. Vakiani, A. Bhalkikar, B.T. Li, F. Di Nicolantonio, A. Bardelli, S. Misale

Writing, review, and/or revision of the manuscript: V. Amodio, R. Yaeger, Y. Bian, S. Marsoni, S. Siena, A. Bertotti, L. Trusolino, B.T. Li, N. Rosen, F. Di Nicolantonio, A. Bardelli, S. Misale

Administrative, technical, or material support (i.e., reporting or organizing data, constructing databases): C. Cancelliere, A. Lorenzato, A. Whaley, H.-Y. Zhao, N. Rosen

Study supervision: V. Amodio, F. Di Nicolantonio, A. Bardelli, S. Misale

Acknowledgments

The authors thank Drs. Maurizio Scaltriti and David Solit for critical reading of the manuscript. The authors also thank the Molecular Cytology Core Facility at MSKCC for technical support. This work was supported by AIRC, Associazione Italiana per la Ricerca sul Cancro, Investigator Grants 20697 (to A. Bertotti), 21407 (to F. Di Nicolantonio), and 22802 (to L. Trusolino), AIRC IG 2018-ID 21923 project-PI Bardelli Alberto, AIRC under 5 per Mille 2018-ID 21091 program: principal investigator A. Bardelli, G.L. A. Bertotti, G.L. F. Di Nicolantonio, G.L. S. Marsoni, G.L. S. Siena, G.L. L. Trusolino, European Research Council Consolidator Grant 724748 – BEAT (to A. Bertotti), H2020 grant agreement no. 754923 COLOSSUS (to L. Trusolino), H2020 INFRAIA grant agreement no. 731105 EDIReX (to A. Bertotti), AIRC/CRUK/FC AECC Accelerator Award 22795 (to A. Bardelli and L. Trusolino), Fondazione Piemontese per la Ricerca sul Cancro-ONLUS, 5 × 1000 Ministero della Salute 2015 Project "STRATEGY" (to F. Di Nicolantonio), Fondazione Piemontese per la Ricerca sul Cancro-ONLUS, and 5 × 1000 Ministero della Salute 2015 Project "IMMUNOGENOMICA" (to A. Bardelli and L. Trusolino), 2014 and 2016 (to L. Trusolino). A. Bertotti and L. Trusolino are members of the EurOPDX Consortium. AIRC MFAG 2017 ID 20236 (to S. Arena). This work was also supported by the NIH R01 CA233736 (to R. Yaeger) and Cancer Center Core Grant P30 CA008748. This research is the responsibility of the authors and does not necessarily represent the official views of the NIH.

The costs of publication of this article were defrayed in part by the payment of page charges. This article must therefore be hereby marked *advertisement* in accordance with 18 U.S.C. Section 1734 solely to indicate this fact.

Received February 17, 2020; revised April 13, 2020; accepted April 29, 2020; published first May 19, 2020.

REFERENCES

1. Zehir A, Benayed R, Shah RH, Syed A, Middha S, Kim HR, et al. Mutational landscape of metastatic cancer revealed from prospective clinical sequencing of 10,000 patients. Nat Med 2017;23:703–13.
2. Simanshu DK, Nissley DV, McCormick F. RAS proteins and their regulators in human disease. Cell 2017;170:17–33.
3. Bos JL, Rehmann H, Wittinghofer A. GEFs and GAPs: critical elements in the control of small G proteins. Cell 2007;129:865–77.
4. Schubbert S, Shannon K, Bollag G. Hyperactive Ras in developmental disorders and cancer. Nat Rev Cancer 2007;7:295–308.
5. Yuan TL, Amzallag A, Bagni R, Yi M, Afghani S, Burgan W, et al. Differential effector engagement by oncogenic KRAS. Cell Rep 2018;22:1889–902.
6. Hunter JC, Manandhar A, Carrasco MA, Gurbani D, Gondi S, Westover KD. Biochemical and structural analysis of common cancer-associated KRAS mutations. Mol Cancer Res 2015;13:1325–35.
7. Ostrem JM, Peters U, Sos ML, Wells JA, Shokat KM. K-Ras(G12C) inhibitors allosterically control GTP affinity and effector interactions. Nature 2013;503:548–51.
8. Lito P, Solomon M, Li LS, Hansen R, Rosen N. Allele-specific inhibitors inactivate mutant KRAS G12C by a trapping mechanism. Science 2016;351:604–8.
9. Patricelli MP, Janes MR, Li LS, Hansen R, Peters U, Kessler LV, et al. Selective inhibition of oncogenic KRAS output with small molecules targeting the inactive state. Cancer Discov 2016;6:316–29.
10. Misale S, Fatherree JP, Cortez E, Li C, Bilton S, Timonina D, et al. KRAS G12C NSCLC models are sensitive to direct targeting of KRAS in combination with PI3K inhibition. Clin Cancer Res 2019;25:796–807.
11. Lou K, Steri V, Ge AY, Hwang YC, Yogodzinski CH, Shkedi AR, et al. KRAS(G12C) inhibition produces a driver-limited state revealing collateral dependencies. Sci Signal 2019;12:pii:eaaw9450.
12. Molina-Arcas M, Moore C, Rana S, van Maldegem F, Mugarza E, Romero-Clavijo P, et al. Development of combination therapies to maximize the impact of KRAS-G12C inhibitors in lung cancer. Sci Transl Med 2019;11:pii:eaaw7999.
13. Xue JY, Zhao Y, Aronowitz J, Mai TT, Vides A, Qeriqi B, et al. Rapid non-uniform adaptation to conformation-specific KRAS(G12C) inhibition. Nature 2020;577:421–5.
14. Canon J, Rex K, Saiki AY, Mohr C, Cooke K, Bagal D, et al. The clinical KRAS(G12C) inhibitor AMG 510 drives anti-tumour immunity. Nature 2019;575:217–23.
15. Hallin J, Engstrom LD, Hargis L, Calinisan A, Aranda R, Briere DM, et al. The KRAS(G12C) inhibitor MRTX849 provides insight toward therapeutic susceptibility of KRAS-mutant cancers in mouse models and patients. Cancer Discov 2020;10:54–71.
16. Prahallad A, Heynen GJ, Germano G, Willems SM, Evers B, Vecchione L, et al. PTPN11 is a central node in intrinsic and acquired resistance to targeted cancer drugs. Cell Rep 2015;12:1978–85.
17. Corcoran RB, Ebi H, Turke AB, Coffee EM, Nishino M, Cogdill AP, et al. EGFR-mediated re-activation of MAPK signaling contributes to insensitivity of BRAF mutant colorectal cancers to RAF inhibition with vemurafenib. Cancer Discov 2012;2:227–35.
18. Yaeger R, Yao Z, Hyman DM, Hechtman JF, Vakiani E, Zhao H, et al. Mechanisms of acquired resistance to BRAF V600E inhibition in colon cancers converge on RAF dimerization and are sensitive to its inhibition. Cancer Res 2017;77:6513–23.
19. Lake D, Correa SA, Muller J. Negative feedback regulation of the ERK1/2 MAPK pathway. Cell Mol Life Sci 2016;73:4397–413.
20. De Robertis M, Loiacono L, Fusilli C, Poeta ML, Mazza T, Sanchez M, et al. Dysregulation of EGFR pathway in EphA2 cell subpopulation significantly associates with poor prognosis in colorectal cancer. Clin Cancer Res 2017;23:159–70.
21. Di Nicolantonio F, Arena S, Gallicchio M, Zecchin D, Martini M, Flonta SE, et al. Replacement of normal with mutant alleles in the genome of normal human cells unveils mutation-specific drug responses. Proc Natl Acad Sci U S A 2008;105:20864–9.
22. Misale S, Yaeger R, Hobor S, Scala E, Janakiraman M, Liska D, et al. Emergence of KRAS mutations and acquired resistance to anti-EGFR therapy in colorectal cancer. Nature 2012;486:532–6.
23. Diaz LA Jr, Williams RT, Wu J, Kinde I, Hecht JR, Berlin J, et al. The molecular evolution of acquired resistance to targeted EGFR blockade in colorectal cancers. Nature 2012;486:537–40.
24. Misale S, Arena S, Lamba S, Siravegna G, Lallo A, Hobor S, et al. Blockade of EGFR and MEK intercepts heterogeneous mechanisms of acquired resistance to anti-EGFR therapies in colorectal cancer. Sci Transl Med 2014;6:224ra26.
25. Bertotti A, Migliardi G, Galimi F, Sassi F, Torti D, Isella C, et al. A molecularly annotated platform of patient-derived xenografts ("xenopatients") identifies HER2 as an effective therapeutic target in cetuximab-resistant colorectal cancer. Cancer Discov 2011;1:508–23.
26. Lazzari L, Corti G, Picco G, Isella C, Montone M, Arcella P, et al. Patient-derived xenografts and matched cell lines identify pharmacogenomic vulnerabilities in colorectal cancer. Clin Cancer Res 2019;25:6243–59.
27. Bertotti A, Papp E, Jones S, Adleff V, Anagnostou V, Lupo B, et al. The genomic landscape of response to EGFR blockade in colorectal cancer. Nature 2015;526:263–7.
28. Serna G, Ruiz-Pace F, Cecchi F, Fasani R, Jimenez J, Thyparambil S, et al. Targeted multiplex proteomics for molecular prescreening and biomarker discovery in metastatic colorectal cancer. Sci Rep 2019;9:13568.
29. Chung KY, Shia J, Kemeny NE, Shah M, Schwartz GK, Tse A, et al. Cetuximab shows activity in colorectal cancer patients with tumors that do not express the epidermal growth factor receptor by immunohistochemistry. J Clin Oncol 2005;23:1803–10.
30. Kopetz S, Grothey A, Yaeger R, Van Cutsem E, Desai J, Yoshino T, et al. Encorafenib, binimetinib, and cetuximab in BRAF V600E-mutated colorectal cancer. N Engl J Med 2019;381:1632–43.
31. Grossmann KS, Rosario M, Birchmeier C, Birchmeier W. The tyrosine phosphatase Shp2 in development and cancer. Adv Cancer Res 2010;106:53–89.
32. Ryan MB, Fece de la Cruz F, Phat S, Myers DT, Wong E, Shahzade HA, et al. Vertical pathway inhibition overcomes adaptive feedback resistance to KRASG12C inhibition. Clin Cancer Res 2020;26:1633–43.
33. Troiani T, Napolitano S, Della Corte CM, Martini G, Martinelli E, Morgillo F, et al. Therapeutic value of EGFR inhibition in CRC and NSCLC: 15 years of clinical evidence. ESMO Open 2016;1:e000088.
34. Saltz LB, Meropol NJ, Loehrer PJ Sr, Needle MN, Kopit J, Mayer RJ. Phase II trial of cetuximab in patients with refractory colorectal cancer that expresses the epidermal growth factor receptor. J Clin Oncol 2004;22:1201–8.
35. Van Cutsem E, Peeters M, Siena S, Humblet Y, Hendlisz A, Neyns B, et al. Open-label phase III trial of panitumumab plus best supportive care compared with best supportive care alone in patients with chemotherapy-refractory metastatic colorectal cancer. J Clin Oncol 2007;25:1658–64.
36. Diaz-Serrano A, Gella P, Jimenez E, Zugazagoitia J, Paz-Ares Rodriguez L. Targeting EGFR in lung cancer: current standards and developments. Drugs 2018;78:893–911.
37. Kuo T, Fisher GA. Current status of small-molecule tyrosine kinase inhibitors targeting epidermal growth factor receptor in colorectal cancer. Clin Colorectal Cancer 2005;5:S62–70.
38. Hembrough T, Thyparambil S, Liao WL, Darfler MM, Abdo J, Bengali KM, et al. Application of selected reaction monitoring for multiplex quantification of clinically validated biomarkers in formalin-fixed, paraffin-embedded tumor tissue. J Mol Diagn 2013;15:454–65.
39. Catenacci DV, Liao WL, Thyparambil S, Henderson L, Xu P, Zhao L, et al. Absolute quantitation of Met using mass spectrometry for clinical application: assay precision, stability, and correlation with MET gene amplification in FFPE tumor tissue. PLoS One 2014;9:e100586.